

Dusty Acoustic Turbulence in the Nuclear Disks of two LINER Galaxies NGC 4450 and NGC 4736

Debra Meloy Elmegreen

*Vassar College, Dept. of Physics & Astronomy, Box 745, Poughkeepsie, NY 12604;
elmegreen@vassar.edu*

Bruce G. Elmegreen

*IBM Research Division, T.J. Watson Research Center, P.O. Box 218, Yorktown Heights,
NY 10598, USA, bge@watson.ibm.com*

Kate S. Eberwein

*Vassar College, Dept. of Physics & Astronomy, Box 745, Poughkeepsie, NY 12604,
kaeberwein@yahoo.com*

ABSTRACT

The structure of dust spirals in the nuclei of the SAab-type Liner galaxies NGC 4450 and NGC 4736 is studied using archival HST PC images. The spirals are typically only several hundredths of a magnitude fainter than the neighboring disks, so unsharp mask techniques are used to highlight them. The ambient extinction is estimated to be less than 0.1 mag from the intensity decrements of the dust features and from the spiral surface filling factor, which is about constant for all radii and sizes. The nuclear dust spirals differ from main-disk spirals in several respects: the nuclear spirals have no associated star formation, they are very irregular with both trailing and leading components that often cross, they become darker as they approach the center, they completely fill the inner disks with a constant areal density, making the number of distinct spirals (the azimuthal wavenumber m) increase linearly with radius, and their number decreases with increasing arm width as a power law. Fourier transform power spectra of the spirals, taken in the azimuthal direction, show a power law behavior with a slope of $-5/3$ over the range of frequencies where the power stands above the pixel noise. This is the same slope as that found for the one-dimensional power spectra of HI emission in the Large Magellanic Cloud, and also the slope expected for a thin turbulent disk. All of these properties suggest that the dust spirals are a manifestation of acoustic turbulence in the inner gas disks of these galaxies. Such turbulence should dissipate orbital energy and transfer angular momentum outward, leading to a steady accretion of gas toward the nucleus.

Subject headings: turbulence — extinction — ISM: structure — galaxies: active
— galaxies: nuclei

1. Introduction

Dust spirals in the inner kpc regions of galaxies reveal a source of compression that can affect the angular momentum distribution of the gas and possibly drive accretion to an AGN. Barred galaxies with an inner Lindblad resonance tend to have two long and symmetric dust spirals near the resonance that are a continuation of the leading-edge dust lanes in the bar (Athanasoula 1992). Many barred galaxies have ILR rings too (Buta & Crocker 1993; Pérez-Ramírez et al. 2000; Knapen et al. 2000). Non-barred galaxies, galaxies without an ILR (e.g., late Hubble types), and regions of barred galaxies inside their ILRs can have more irregular dust spirals.

Whether the nuclear spirals are regular or irregular, their presence in optical images suggests a density variation that is at least a factor of 2 and therefore likely to involve shocks. These shocks are oblique for azimuthal flows, so the gas will experience a torque when it enters a spiral and an opposite torque when it leaves. In cases where the gas moves faster than the spirals, the net torque is negative and the gas loses angular momentum and energy at the shock, causing it to spiral inward. If the spirals move faster than the gas, as might be the case outside a fast nuclear bar, then the gas gains angular momentum and may gradually move out.

We are interested in the source of compression for the irregular nuclear dust spirals that appear in non-barred galaxies or inside the ILRs of some barred galaxies. We have proposed that some of these are caused by random sonic noise that amplifies weakly as it propagates toward the center (Elmegreen et al. 1998; Montenegro, Yuan, & Elmegreen 1999; Englmaier & Shlosman 2000). A signature of this process is an irregularity of structure, a wide range of pitch angles reflecting different times of origin and different wave propagation directions, a tendency to fill the volume available with a spiral separation comparable to the epicyclic radius for motions at the sound speed, and a general trend of increasing density with decreasing radius for each spiral. Because the velocities inside these spirals cannot yet be measured, there is no way to be sure they are driving inflow. Nevertheless, if any of the spirals come close to the nucleus, then such accretion would seem to be likely.

Nuclear dust spirals and clouds have been studied previously using Hubble Space Telescope (HST) data. Van Dokkum & Franx (1995) found them on WFPC V-band images of early type galaxies. Malkan, Gorjian, & Tam (1998) did a large snapshot survey of active

galaxies and classified the nuclear morphology including the dust. Elmegreen et al. (1998) noted dust spirals in WFPC2 images of the interacting galaxy NGC 2207 and proposed they might drive accretion to the nucleus. Regan & Mulchaey (1999) found nuclear dust spirals in 6 AGN galaxies using WFPC2 and NICMOS images, and Martini & Pogge (1999) found them with HST data in 20 Seyferts; both studies concluded that the spirals could drive accretion. Ferruit, Wilson & Mulchaey (2000) studied 12 early type Seyfert galaxies in more detail and noted the dust spirals too. Tomita et al. (2000) used HST archival images to study dust features in E and S0 galaxies, but did not comment on spirals specifically. Tran et al. (2001) studied nuclear dust in elliptical galaxies.

Here we measure the extinction and structural properties of irregular dust spirals in the central kpc of two LINER galaxies, NGC 4450 and NGC 4736. Their Hubble types are about the same, SA(s)ab and RSA(r)ab (de Vaucouleurs et al. 1991), and their distances are taken to be 16.8 and 4.3 Mpc (Tully 1988).

2. Observations

Hubble Space Telescope preview images of the galaxies NGC 4450 and NGC 4736 are shown in Figure 1. These images were obtained from the HST archive web site and are degraded in resolution by a factor of 2 from the full HST data; they are from proposals 5375 by V. Rubin and 5741 by J. Westphal, respectively. For our analysis of dust structure, we used the original Planetary Camera (PC) images with $0.0455''$ per pixel, corresponding to 3.7 pc and 0.95 pc per pixel, respectively. The PC fields of view cover 3000 pc and 760 pc. Multiple images in the V passband (F555W filter) were combined to remove cosmic ray tracks and bad pixels. Figure 1 shows the full WFPC2 image to illustrate the outer disk morphologies, their position angles, and the orientation of the HST images relative to north.

2.1. Dust Absorption

Intensity decrements for dust cloud absorption were measured for many features using radial and azimuthal profiles on the PC images. Figure 2 shows a sample profile from the V-band image of NGC 4736 taken along the strip shown in Figure 3 (which uses the G4-G12 enhanced image from Fig. 6 below). Most of the intensity dips deeper than a few hundredths of a magnitude are dust features, as can be determined by comparing Figures 2 and 3. The thinner features may be verified as dust also by comparing Figure 2 with the G1-G3 and G2-G6 images in Figure 6.

Intensity decrements do not measure the cloud extinction because there is likely to be a smooth intensity contribution from foreground starlight. If dust with opacity τ in the midplane is next to an intercloud medium with opacity τ_0 , then the cloud to intercloud intensity ratio is $(1 + e^{-\tau}) / (1 + e^{-\tau_0})$. For $\tau > \tau_0$, this ratio is between 0.5 and 1, making the maximum cloud contrast 0.75 mag. Thus the magnitude difference is not a good measure of intrinsic extinction unless τ is small and τ_0 is either independently known or close to zero. An intensity ratio lower than 0.5 corresponds to an opaque dust cloud on the near side of the galaxy.

Radiative transfer models of the intensity distributions in several passbands are necessary to determine the intrinsic opacities of these clouds, but the present HST data were not acquired for this purpose and the wavelength coverage and integration times are not adequate for a proper analysis. Dust spirals in another, similar, nuclear region were analyzed by radiative transfer previously using HST data in V and I passbands (Elmegreen et al. 1998). We found that typical extinctions are several magnitudes inside the darkest clouds, and that the average extinction in the inner disk is so low that the gas is not likely to be self-gravitating. We expect the same situation here because of a lack of star formation associated with the dust. Radiative transfer models of dust features for main galaxy disks are more common than for nuclear disks (e.g., Howk & Savage 1997; Kuchinski et al. 1998; Regan 2000). Galaxy extinctions have also been measured using background sources (e.g., Pizagno & Rix 1998; White, Keel, & Conselice 2000; Keel & White 2001; Elmegreen et al. 2001)

The typical absorption trough for a dust feature in Figure 2 is several hundredths of a magnitude in V band. The deep feature indicated is part of a long dust spiral that covers a factor of two in radius and then branches into two thinner spirals in the inner part (see Fig. 3). Figure 4 shows the magnitude difference for this spiral and several others in the two galaxies as a function of radius. These differences were measured by comparing the intensities of the dust lanes to the adjacent interdust regions at several radii. Estimated measuring uncertainties are 0.002 mag. Each line in Figure 4 is a different spiral; the top dashed line corresponds to the dust feature shown in Figure 2. The darkness of the dust generally increases inward, suggesting that either the density of the spirals or their thickness relative to the stellar disk increases inward.

2.2. Image Enhancement, Fractal Structure, and Dust Opacity

The spiral dust structures are very faint. They require enhancement with unsharp masks or other filtering techniques. Figures 5 and 6 show composites of four filtered images for

each galaxy. Each filter isolates structures within a range of scales spanning a factor of 3. The top left panels contain unsharp-masked images made by subtracting a smoothed version from the original image, using a smoothing function that is a Gaussian with a dispersion of $\sigma = 3$ pixels. This image shows the smallest structures, from 1 to 3 pixels. In the top right, a smoothed image with a $\sigma = 6$ px Gaussian was subtracted from a smoothed image with a $\sigma = 2$ px Gaussian (this will be called a G2-G6 image). This shows features with scales between 2 px and 6 px. The bottom left and right images subtract $\sigma = 12$ px from $\sigma = 4$ px convolutions (G4-G12) and $\sigma = 24$ px from $\sigma = 8$ px convolutions (G8-G24), respectively. Each image has considerable structure, indicating that clouds span a wide range of scales.

The fractal dimension of multiscale structure can be determined from box counting or cloud counting techniques, plotting the number of structures as a function of scale in log-log coordinates (Mandelbrot 1982; Westpfahl et al. 1999). Because we have already isolated certain scales with each filter, the cloud counting results on the subtracted images will give the same slope as the derivative with respect to length of the box counting results on the original images. Recall that box counting includes all structures larger than the scale of the box. The fractal dimension D is the slope of the function $N(> S)$ versus S on log-log coordinates for number of structures larger than S determined by the box counting technique. If we write $N(> S) = \int_S^\infty n(S)dS$ for number of structures $n(S)$ between S and $S + dS$, then $n(S)dS \propto S^{-D-1}dS$ and $n(S)d \log S \propto S^{-D}d \log S$ for linear and log intervals of size, respectively. Thus the slope on a log-log plot of the number of clouds in each interval of filter size, for logarithmically spaced intervals like we have in Figures 5 and 6, gives the fractal dimension of the cloud structures. We choose the filter technique rather than the box technique so we can see the nature of the structure on each scale, whether it is filamentary or shell-like, for example. Figures 5 and 6 indicate that it is filamentary on all the resolved scales.

Figure 7 shows the number of spirals intercepted by deprojected azimuthal scans on the G2-G6 image plotted as a function of radius. The radii used for the measurements are 22, 45, 67, 90, and 112 pixels. A deprojected azimuthal scan of this image showing average counts for the radial interval from 66 to 68 pixels is shown in Figure 8. The number of clouds plotted in Figure 7 at this radius, 22 clouds, is shown again in Figure 8, with each cloud indicated by an arrow. The full circle of the azimuth in Figure 8 corresponds to 421 pixels. Generally the cloud count can be done easily by eye on a computer screen down to the brightness limit of the image. The number of dark features in an azimuthal scan is always about one-third of the radius, which makes the azimuthal spacing between them $\sim 6\pi$ pixels. Because the average cloud size on this image is ~ 4 px, the clouds fill $4/(6\pi) = 21\%$ of the circumference.

This spiral filling factor makes sense given the extinction contrast. If the spirals formed

by the compression of a fraction f of the gas and the spiral spacing is $C \sim 5$ times the spiral width (C is the inverse of the filling factor given above), then the column density of each spiral is $(C - 1)f + 1$ times the ambient average. This column density has a contribution from uncompressed material that was at the spiral position already, which is the fraction $1 - f$ of the ambient column density, plus the compressed material from the whole volume out to the next spiral, which is the amount fC times the ambient column density. The sum is $1 - f + fC = (C - 1)f + 1$ times the ambient column density, as above. The assumption here is that not all of the interstellar medium will be compressed by the turbulence. A warm or hot component, with a thermal speed larger than the mean turbulent speed, should flow around the moving clouds and not compress easily. Thus f may be considered the mass fraction of the gas that is compressible by the prevailing turbulence.

In this situation, suppose the spiral opacity is τ , the interspiral opacity is τ_0 , and the ambient average before the compression was τ_a , all from gas concentrated in the mid-plane. Then the compression gives $\tau = [(C - 1)f + 1]\tau_a$, the conservation of mass gives $\tau + (C - 1)\tau_0 = C\tau_a$, and the density contrast in magnitudes, Δm , gives

$$\frac{1 + e^{-\tau}}{1 + e^{-\tau_0}} = 10^{-0.4\Delta m} \quad (1)$$

These equations can be solved for the three opacities given C , f , and Δm . This solution has a simple expression in the limit of small Δm . In that case, there are two solutions for τ , τ_0 and τ_a , one where the opacities are very large so hardly any background light gets through, and another where the opacities are very small. The relatively smooth continuation of the outer disk starlight into the inner region implies the latter. Then in the limit of small Δm ,

$$\tau_a \sim 0.8 \ln 10 \Delta m / (fC). \quad (2)$$

For $C \sim 5$ and $f \sim 1/2$, this gives $\tau_0 \sim 0.7\Delta m$ on average. Considering $\Delta m \sim 0.04$ from Figure 4, the ambient opacity of $\tau_a \sim 0.03$ corresponds to a mass column density of $\sim 0.5 M_\odot \text{ pc}^{-2}$. This result is ~ 10 times smaller than the average extinction in the center of NGC 2207, which was about 0.6 mag (Elmegreen et al. 1998), but the dust features here are ten times fainter than in NGC 2207, where a prominent dust lane used for the opacity measurement had a V-band intensity contrast of 0.3 mag. Evidently, the column densities in NGC 4450 and NGC 4736 are too small for the inner gas disks to be significantly self-gravitating; for reasonable epicyclic frequency and velocity dispersion, the Toomre stability parameter Q exceeds 100.

We can do this same exercise for spirals of different sizes. The top part of Figure 9 shows the number of dust spirals counted in different azimuthal scans versus the size of the Gaussian filter, plotting the G1-G3 filter combination as a point with an average Gaussian

radius of 2, for example. The radii used for the azimuthal scans are 45, 67, 90 and 112 pixels. The number of dust spirals decreases approximately inversely with Gaussian filter radius for all galactic radii, suggesting again that the spirals are packed in tightly, even on a variety of scales. If the spacing between spirals in the azimuthal direction is λ , and this spacing is the factor C times the spiral width, W , then the number N of spirals at radius R is $2\pi R/\lambda$ and the inverse of the filling factor is $C = 2\pi R/(NW)$. This inverse filling factor, C , is shown in the bottom of Figure 9. For all but the smallest features, which are probably undercounted, $C \sim 3 - 5$ for all sizes and radii. This is the same value of C that was used in the previous discussion of τ_a . Thus the spirals are likely to be made on a wide variety of scales by *compressions* of a factor of $C \sim 3 - 5$ from an ambient medium with an opacity slightly less than 0.1 mag. We suggest below that the mean gas density could be $\sim 1.5 \text{ cm}^{-3}$.

The top part of Figure 9 may also be used to determine a fractal dimension, which equals the slope according to the discussion at the beginning of this subsection. The number of clouds decreases a little less rapidly than the inverse of the smoothing scale σ , giving an apparent fractal dimension slightly less than 1. If we write the dependence of the number of counted clouds on the cloud size as a power law, σ^{-D} , for logarithmic intervals of σ , then D is the fractal dimension. From Figure 9, D equals 0.79 ± 0.16 for NGC 4450 and 0.51 ± 0.04 for NGC 4736, considering Gaussian radii from 4 to 32.

2.3. Fourier Transform Power Spectra

Fourier transform power spectra of the azimuthal intensity profiles at ten radii in each galaxy are shown in Figure 10. The radii R were chosen so that $2\pi R$ equals an allowable number of pixels in a Fast Fourier Transform done with the SRCFT subroutine in the IBM ESSL software package. These numbers give radii $R = 33, 57, 81, 107, 134, 153, 183, 204, 229$, and 244 pixels.

The power spectra are the sums of the squared real and imaginary parts of the FFTs. These are one-dimensional FFTs, taken from the azimuthal intensity traces along the de-projected images. Deprojection was made with a position angle of 7° and an inclination of 42.2° for NGC 4450 on the HST image, and with a position angle and inclination of -2° and 35.6° for NGC 4736. The inclinations were taken from the Third Reference Catalogue of Bright Galaxies (de Vaucouleurs et al., 1991). The position angles were measured from the HST images of the nuclear regions and differ from the position angles of the outer disks. In terms of the number of degrees counter-clockwise from North, the position angles of the nuclear-disk major axes are $\sim 1^\circ$ and $\sim 21^\circ$ for NGC 4450 and NGC 4736, respectively.

The projected ellipses used for the intensity traces are shown on the G4-G12 images in Figure 11. Each intensity trace is an average over 9 deprojected azimuthal scans spaced by one pixel and centered on one of the radii R given above. Each pixel used for an azimuthal average is blackened in Figure 11.

The power spectra are illustrated in Figure 10 by stacking the different radii on top of each other with the smallest radius at the bottom. The vertical scale corresponds to a factor of 10 in the power spectrum for each tic mark; the absolute scale is arbitrary. The solid, dashed, and dot-dashed lines have slopes of $-5/3$, -1 , and $-8/3$. Solid lines with a slope of $-5/3$ are drawn through the low frequency portions of each power spectrum to illustrate the general trend.

The power spectra all have slopes of about $-5/3$ at low frequency. The slopes flatten at high frequency to a slope of about -1 or flatter. The low frequency power spectrum could be steeper than $-5/3$ at the smallest radius, possibly as steep as $-8/3$, as shown by the dot-dashed line.

Turbulence gives a one-dimensional power spectrum with a slope of $-5/3$ for structures that are thinner on the line-of-sight than the transverse wavelength, and a slope of $-8/3$ for structures that are thicker on the line-of-sight than the wavelength (Lazarian & Pogosyan 2000). Two-dimensional power spectra have slopes for these two cases that are steeper by one, i.e., $-8/3$ and $-11/3$. The azimuthal scan results here, giving slopes of $-5/3$ at small spatial frequencies, are consistent with turbulent structures that are wider than the galaxy disk scale height.

The same slope of $-5/3$ was found for power spectra of azimuthal scans of the HI intensity of the Large Magellanic Cloud (Elmegreen, Kim, & Staveley-Smith 2001). Thus the origin of the structure is probably the same. Power law power spectra have also been found in other interstellar emission line surveys, using HI (Crovisier & Dickey 1983; Green 1993) and CO (Stutzki et al. 1998) in the Milky Way and HI in the Small Magellanic Cloud (Stanimirovic et al. 1999). The slopes are always consistent with turbulence as the origin of the structure.

The LMC showed a turnover in the power spectrum at high spatial frequency in both the azimuthal and linear scans, going from slopes of $-5/3$ to $-8/3$ at high spatial frequency, and it showed a similar turnover in the two-dimensional power spectrum of the whole disk, going from $-8/3$ to $-11/3$ at high frequency. These turnovers were proposed to correspond to the transition from structures that are larger in the transverse direction than the galaxy thickness to structures that are smaller than the galaxy thickness (Elmegreen, Kim, & Staveley-Smith 2001), as predicted in the general case by Lazarian & Pogosyan (2000). Elmegreen et al. also

found that LMC thickness increased with radius. This result was confirmed by Padoan et al. (2001), who found a similar thickness-dependent feature in the spectral correlation function of HI emission from the LMC, and used this feature to map the inferred disk thickness around the plane. Analogous turnovers in the power spectrum are not seen for the nuclear dust spirals studied here, presumably because the noise level is too high. This problem is suggested by the flattening of the power spectra at intermediate to high frequencies – before the turnover can occur. Longer integration times on these sources could possibly get the noise down to a level where the power spectrum turns over. Then the line-of-sight disk thicknesses could be measured. All we can say here is that the thickness is less than ~ 50 pc in NGC 4450 and less than ~ 10 pc in NGC 4736. These limits are not unreasonable because they can still give the inner gas disks about the same aspect ratios as a typical main galaxy gas disk. When combined with the average extinction estimate given in the previous subsection, $A_V \sim 0.03$ mag, a disk thickness of ~ 10 pc corresponds to an average gas density of $\sim 1.5 \text{ cm}^{-3}$, which is about the same as that in the Solar neighborhood.

The morphologies of the dust structures in the nuclear regions of NGC 4450 and NGC 4736 differ from the morphologies of the gas emission structures in the Milky Way and Magellanic Clouds surveys. In the nuclear regions, the dust is mostly in the form of spirals, which show a power-law power spectrum in the azimuthal direction and a gradient of intensity in the radial direction (cf. Fig. 4). For the HI and CO emission line surveys, the structures are more blob-like or shell-like, with essentially no spirals, even in the whole LMC and SMC. Evidently, the origin of these gaseous structures is the same, i.e., random and persistent compressions from turbulence, but the nuclear regions of NGC 4450 and NGC 4736 have a lot of shear also, and this shear distorts the compressed regions into spirals. The LMC and SMC have relatively little shear, as do local interstellar clouds.

Numerical simulations of this shearing effect for gravitating media were in Toomre & Kaljnas (1991), Huber & Pfenniger (1999), Wada & Norman (1999), and Semelin & Combes (2000). Pressures from star formation were also considered by Wada, Spaans, & Kim (2000) and Wada & Norman (2001). The present case differs from these others slightly because the nuclear dust structures here are mostly without star formation and they are probably also without significant self-gravity. The origin of the turbulence is unknown, although a mild, pressure-driven instability was suggested by Montenegro et al. (1999).

3. Discussion

The nuclear spirals in NGC 4450 and NGC 4736 vaguely resemble the outer spirals, which are somewhat flocculent in each case, but the nuclear spirals do not continue smoothly

from the outer spirals and there are important structural differences. The B-band image of NGC 4450 in the Carnegie Atlas of Galaxies (Sandage & Bedke 1994) shows two long dust spirals in the main disk, along with some flocculent structure; the stellar spiral arms are smooth. In contrast, the nuclear region has no stellar arms and at least 7 prominent dust arms, some with pitch angles as high as 45° and some crossing each other. The eastern side of the nuclear region shows more dust than the western side because of the galaxy’s inclination. Some small dust feathers extend nearly radially from the center toward the south, reminiscent of jets. HST spectral observations by Ho et al. (2000) reveal double-peaked line profiles with high velocity wings, characteristic of accretion disk activity observed in other LINERs.

NGC 4736 is an early-type galaxy with an outer ring and a circumnuclear starburst ring. Its main disk structure is flocculent and defined primarily by the dust. Sandage & Bedke’s B-band print shows the inner disk structure as composed of many tightly-wrapped arms, but the central region is saturated in the reproduction. Waller et al. (2001) present UIT UV and ground-based R-band images of the central regions, including an unsharp-masked image showing the complicated flocculent structure of the main disk. They also show an HST FOC image of the main nuclear dust arms. Ground-based NIR observations by Mollenhoff, Matthias, & Gerhard (1995) suggested a weak stellar bar with a length of $20''$, which was also noted by Maoz et al. (1995) from an HST FOC image. The bar was observed in CO by Sakamoto et al. (1999) and Wong & Blitz (2000). In the HST image, the region corresponding to the bar shows up as an elongated disk with a position angle nearly perpendicular to the major axis of the galaxy. The structure inside the circumnuclear ring, which is really two tightly wrapped arms, consists of a dozen dust arms within a radius of 50 pc from the center, branching to dozens more dust spirals out to 200 pc. The nuclear dust spirals are not attached to the main inner disk dust spirals.

The nuclear dust in NGC 4450 and NGC 4736 has several characteristics that differ from spiral arms and dust clouds in main galaxy disks. These are:

- The nuclear dust spirals shown here have no associated star formation. Other nuclear spirals in different galaxies have star formation (e.g., Coma D15 in Caldwell, Rose, & Dendy 1999), so the gaseous nature here is not universal. The lack of star formation suggests that the inner gas disks in NGC 4450 and NGC 4736 are not strongly self-gravitating. The same was true for NGC 2207 (Elmegreen et al. 1998) and for several other inner disks in the study by Martini & Pogge (1999). Our opacity estimate in Section 2.2 is also consistent with this.
- The nuclear dust is in the form of spiral arms of various pitch angles, widths, and lengths. Some of the arms are trailing, a few are leading, and many cross each other.

This pattern is generally more irregular than main disk flocculent arms (see atlas in Elmegreen 1981). Main disk flocculent arms are rarely leading. They generally do not cross each other; if they branch into spurs, then this branching is toward larger radii (Elmegreen 1980). They also have star formation that gives them a thicker, more patchy quality, rather than a filamentary quality.

- The nuclear dust spirals in NGC 4450 and NGC 4736 have decreasing contrast with increasing radius. Ambient dust extinctions generally decrease with galactocentric distance because of the exponential distribution of gas column density. The flocculent galaxy NGC 5055 has such a decrease, for example, as measured by the extinctions of OB associations (Acarreta et al. 1996). Nuclear dust spirals are not just ambient extinctions, however. They are morphologically more similar to main disk spiral arms than diffuse cloud extinctions because they are organized and most likely formed by compressive processes in the presence of shear. From this point of view, nuclear dust spirals should be compared to main disk spirals, and then the radial decrease in nuclear spiral amplitude is unusual. Density wave spirals in non-barred galaxies tend to get stronger with increasing radius, out to at least the corotation zone (Elmegreen & Elmegreen 1984; Elmegreen et al. 1996). The unusual result that nuclear dust spirals get weaker with radius is presumably the result of crowding near the center for waves that move inward, as predicted for solutions to Bessel’s wave equation (Elmegreen et al. 1998; Montenegro et al. 1999). This is a different dynamical situation than for main disk spiral arms, for which the curvature terms ($\propto 1/kr$ for wavenumber k) in the wave equations can usually be ignored (e.g., Bertin et al. 1989).
- The number density of dust features is about constant with radius, indicating that the inner disk is completely filled with structure. This is unlike the situation for main galaxy disks which often have a small number of arms (e.g., 2-5) that get further apart with radius. The nuclear spirals also have some indication of a hierarchical or fractal structure because of a non-integer slope of the size distribution, examined with unsharp masks. This size distribution is approximately a power law with a slope in the range from 0.5 to 0.8. This power law is reminiscent of other properties of interstellar clouds formed by turbulence, but complicated in this case by the effects of shear, which make spirals rather than clumps, and by the Coriolis force, which resists turbulent motions on large scales. The dust features are also very weak, and the smaller clouds, as well as those further from the center, are difficult to see above the pixel noise. Fractal structure in the dust of another galaxy was also found by Keel & White (2001) using a background illumination source. Fractal structure in galactic clouds is well known (e.g., Falgarone, Phillips, & Walker 1991).

- Fourier transform power spectra in the azimuthal direction show the characteristic signature of turbulence compression, which is a power law slope of $-5/3$ for one-dimensional structures that are larger than the line-of-sight thickness of the galaxy disk. This makes the nuclear dust features studied here resemble the HI clouds in the LMC, with the important difference that the nuclear clouds are spiral filaments, presumably affected by shear, and the LMC clouds are globular and shell-like in a low shear environment.

There is no direct evidence in our observations for accretion driven by the dust spirals. Radial velocities will have to be measured to determine this. However, the increase in dust opacity with decreasing radius for the main spirals is consistent with the amplification that is expected for inward motions. In that case, the spirals could drive nuclear accretion.

D.M.E. and B.G.E. gratefully acknowledge HST archival grant HST-AR-09197. We also acknowledge useful comments by the referee.

REFERENCES

- Acarreta, J.R., Manteiga, M., Pismis, P., Mampaso, A., & Cruz-Gonzalez, G. 1996, *AJ*, 112, 1894
- Athanassoula, E. 1992, *MNRAS*, 259, 345
- Bertin, G., Lin, C.C., Lowe, S.A., & Thurstan, R.P. 1989, *ApJ*, 338, 104
- Buta, R.J., & Crocker, D.A. 1993, *AJ*, 105, 1344
- Caldwell, N., Rose, J.A., & Dendy, K. 1999, *AJ*, 117, 140
- de Vaucouleurs, G., de Vaucouleurs, A., Corwin, H. G., Jr., Buta, R., Paturel, G., & Fouque, P. 1991, *Third Reference Catalogue of Bright Galaxies*, (New York: Springer-Verlag)
- Elmegreen, D.M. 1980, *ApJ*, 242, 528
- Elmegreen, D.M. 1981, *ApJS*, 47, 229
- Elmegreen, B.G., Elmegreen, D.M., Brinks, E., Yuan, C., Kaufman, M., Klaric, M., Montenegro, L., Struck, C., & Thomasson, M. 1998, *ApJL*, 503, L119
- Elmegreen, D.M., & Elmegreen, B.G. 1984, *ApJS*, 54, 127

- Elmegreen, B.G., Elmegreen, D.M., Chromey, F.R., Hasselbacher, D.A., & Bissell, B.A. 1996, *AJ*, 111, 2233
- Elmegreen, D.M., Kaufman, M., Elmegreen, B.G., Brinks, E., Struck, C., Klaric, M., & Thomasson, M. 2001, *AJ*, 121, 182
- Englmaier, P., & Shlosman, I. 2000, *ApJ*, 528, 677
- Falgarone, E., Phillips, T. G., & Walker, C. K. 1991, *ApJ*, 378, 186
- Ferruit, P., Wilson, A. S., & Mulchaey, J. 2000, *ApJS*, 128, 139
- Ho, L.C., Filippenko, A.V., & Sargent, W.L.W. 1997, *ApJ*, 487, 591
- Howk, J.C., & Savage, B.D. 1997, *AJ*, 114, 2463
- Huber, D., & Pfenniger, D. 1999, in *The Evolution of Galaxies on Cosmological Timescale*, eds. J.E. Beckman & T.J. Mahoney, *Astrophysics and Space Science*, poster paper
- Keel, W.C., & White, R.E., III 2001, *AJ*, 121, 1442
- Knapen, J., Shlosman, I., Heller, C. H., Rand, R., Beckman, J., & Rozas, M. 2000, *ApJ*, 528, 219
- Kuchinski, L. E., Terndrup, D. M., Gordon, K. D., & Witt, A. 1998, *AJ*, 115, 1438
- Lazarian, A., & Pogosyan, D. 2000, *ApJ*, 537, 720
- Mandelbrot, B.B. 1982, *The Fractal Geometry of Nature*, (San Francisco: Freeman)
- Maoz, D., Filippenko, A.V., Ho, L.C., Rix, H.-W., Bahcall, J.N., Schneider, D.P., & Macchetto, F.D. 1995, *ApJ*, 440, 91
- Malkan, M.A., Gorjian, V., & Tam, R. 1998, *ApJS*, 117, 25
- Martini, P., & Pogge, R.W. 1999, *AJ*, 118, 2646
- Mollenhoff, C., Matthias, M., & Gerhard, O.E. 1995, *A&A*, 301, 359
- Montenegro, L., Yuan, C., & Elmegreen, B.G. 1999, *ApJ*, 520, 592
- Pérez-Ramírez, D., Knapen, J., Peletier, R., Laine, S., Doyon, R., & Nadeau, D. 2000, *MNRAS*, 317, 234
- Pizagno, J., Rix, H.-W. 1998, *AJ*, 116, 2191

- Regan, M.W. 2000, ApJ, 541, 142
- Regan, M. W., & Mulchaey, J. S. 1999, AJ, 117, 2676
- Sakamoto, K., Okumura, S.K., Ishizuki, S., & Scoville, N.Z. 1999, ApJ Suppl, 124, 403
- Sandage, A., & Bedke, J. 1988, Atlas of Galaxies, U.S. Govt. Printing Office. Washington, D.C., NASA
- Tomita, A., Aoki, K., Watanabe, M., Takata, T., & Ichikawa, S. 2000, AJ, 120, 123
- Toomre, A., & Kalnajs, A.J. 1991, in Dynamics of Disk Galaxies, ed. B. Sundelius, University of Chalmers, p. 341
- Tran, H.D., Tsvetanov, Z., Ford, H.C., Davies, J., Jaffe, W., van den Bosch, F.C., & Rest, A. 2001, AJ, 121, 2928
- Tully, R.B. 1988, Nearby Galaxies Catalog, Cambridge: Cambridge University Press.
- van Dokkum, P.G., & Franx, M. 1995, AJ, 110, 2027
- Wada, K., & Norman, C. A. 1999, ApJ, 516, L13
- Wada, K., & Norman, C. A. 2001, ApJ, 547, 172
- Wada, K., Spaans, M., & Kim, S. 2000, ApJ, 540, 797
- Waller, W. H., Fanelli, M.N., Keel, W.C., Bohlin, R., Collins, N.R., Madore, B.F., Marcum, P.M., Neff, S.G., O’Connell, R.W., Offenberg, J.D., Roberts, M.S., Smith, A.M., & Stecher, T.P. 2001, AJ, 121, 1395
- Westpfahl, D.J., Coleman, P.H., Alexander, J., & Tongue, T. 1999, AJ, 117, 868
- White, R.E., III, Keel, William C., & Conselice, C.J. 2000, ApJ, 542, 761
- Wong, T., & Blitz, L. 2000, ApJ, 540, 771

Fig. 1.— NGC 4450 (left) and NGC 4736 (right) V-band images from HST WFPC2. (See jpeg files in astro-ph.)

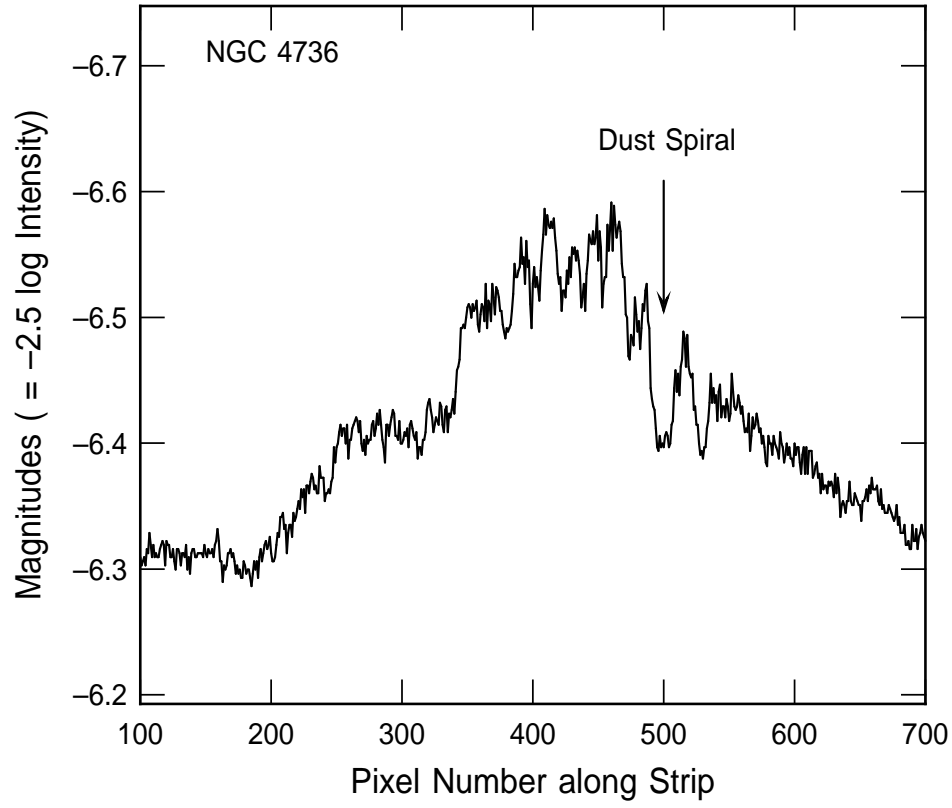


Fig. 2.— An intensity trace across a dust spiral in NGC 4736 showing an absorption dip, which is labeled, and other dust features. The maximum of intensity in the center of the scan is from the exponential disk.

Fig. 3.— The 600-pixel long scan used for Fig. 2 is shown superposed on the G4-G12 image from Fig. 6. The dust is dark in this image. (See jpeg file in astro-ph.)

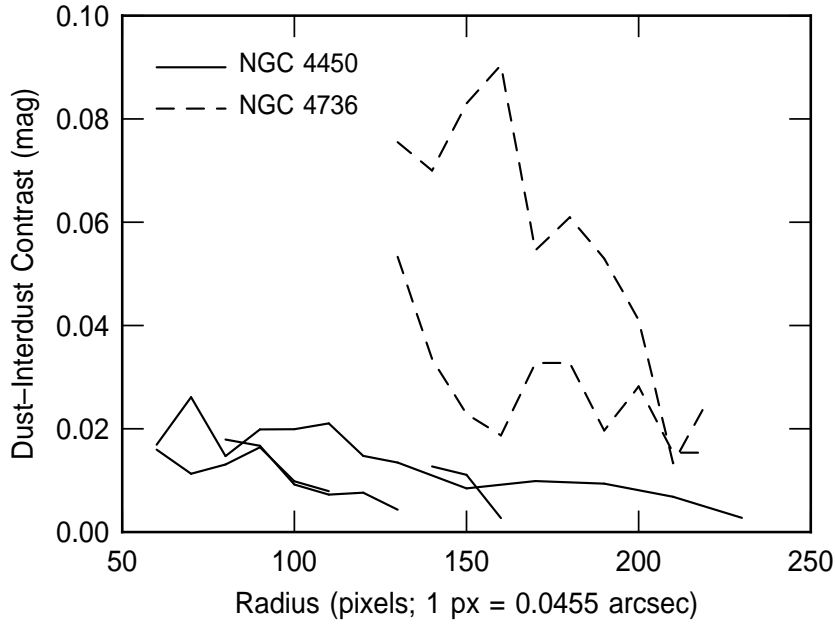


Fig. 4.— The magnitude differences between the dust features and the neighboring interdust regions are plotted versus the distance from the galaxy centers for four dust spirals in NGC 4450 and two dust spirals in NGC 4736. The dust spirals tend to get darker toward the center.

Fig. 5.— Unsharp mask images of NGC 4450, made by subtracting two Gaussian smoothed images, $G_n - G_m$, for Gaussian dispersions n and m , measured in pixels. The top left panel shows $G_1 - G_3$; top right: $G_2 - G_6$; bottom left: $G_4 - G_{12}$, and bottom right: $G_8 - G_{24}$. The number of pixels along the horizontal edge of each image is 725, corresponding to 2700 pc. (See jpeg file in astro-ph.)

Fig. 6.— Unsharp mask images of NGC 4736, as in Fig. 5. The number of pixels along the horizontal edge of each image is 590, corresponding to 560 pc. (See jpeg file in astro-ph.)

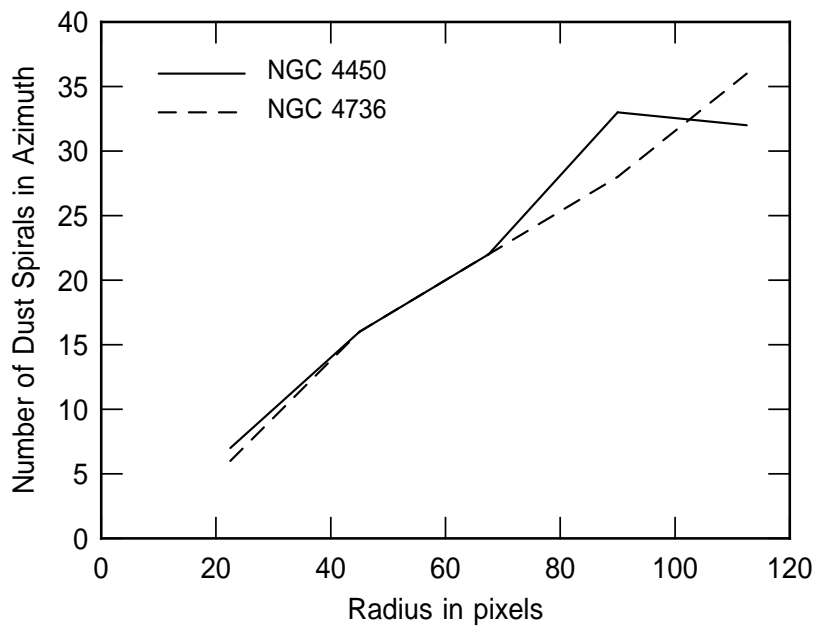


Fig. 7.— The numbers of distinct dust spirals in azimuthal scans on the G2-G6 images are plotted versus the radii. The numbers equal approximately one-third the radii, indicating that the filling factor for the dust is about 0.2 on the scale of ~ 4 pixels.

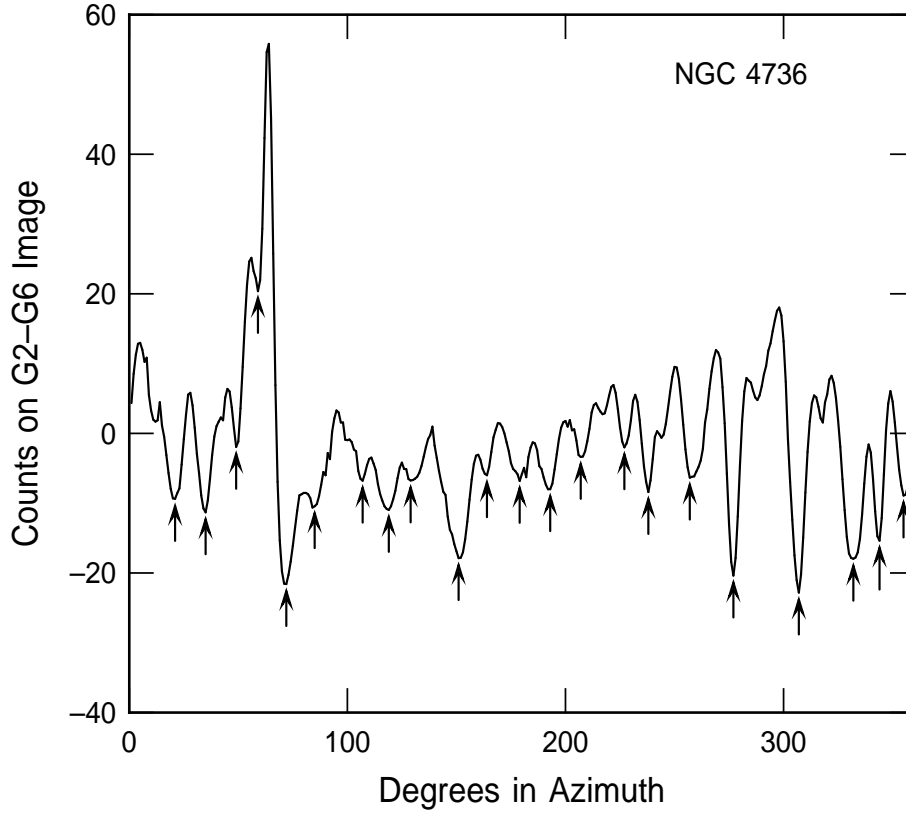


Fig. 8.— A deprojected azimuthal scan at a radius of 67 pixels for the G2-G6 image of NGC 4836 showing dust features as negative counts. The 22 features counted for Figure 7 are indicated. The full azimuth of 360° plotted here corresponds to 421 pixels, so the average spacing between these clouds is $421/22=19$ pixels, which is close to the value of 6π discussed in the text.

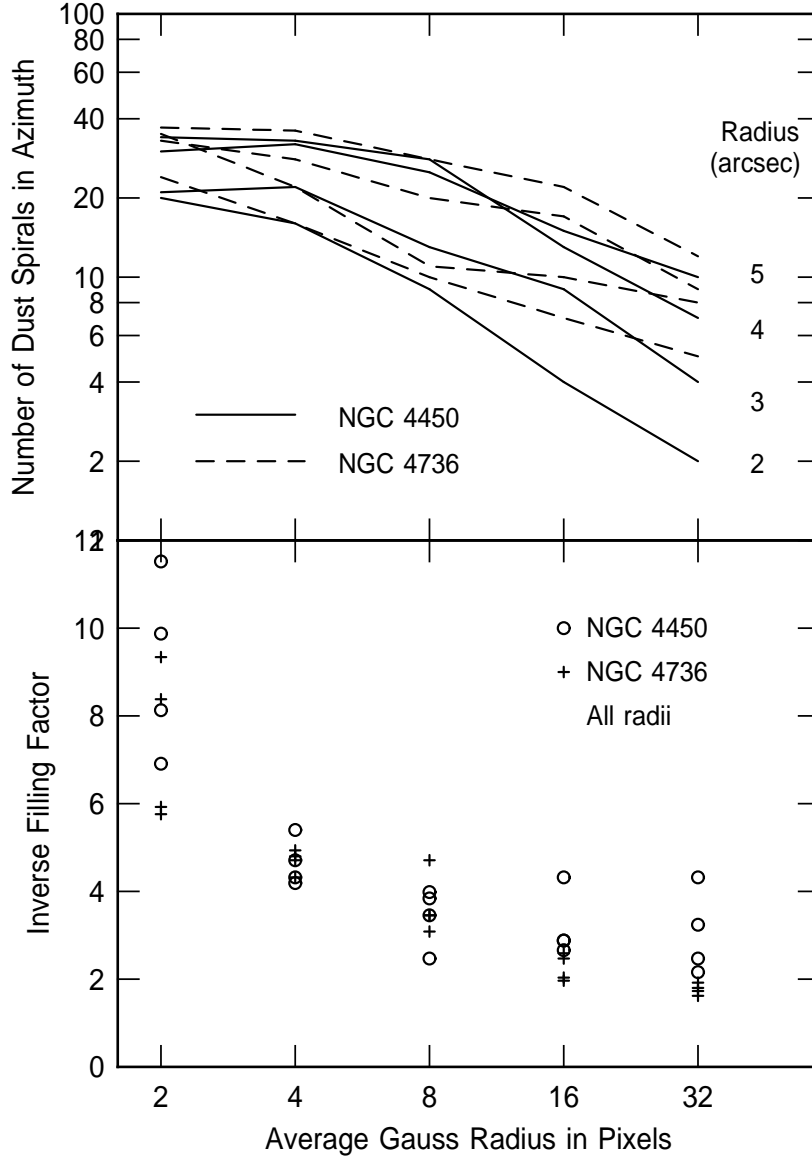


Fig. 9.— (top) The number of distinct dust spirals in azimuthal scans of different radii is shown as a function of the Gaussian dispersion of the unsharp mask, which is the characteristic feature size. The radii for the scans are 45, 67, 90, and 112 pixels. The number of spirals decreases approximately as a power law over a factor of ten in size. The slope of this power law is the fractal dimension. (bottom) The ratio of the azimuthal spacing between the spirals to the spiral width given by the average Gaussian smoothing radius. This ratio is the inverse of the areal filling factor of the spirals, and it is about constant, equal to ~ 4 for all radii and spiral arm widths larger than ~ 4 pixels.

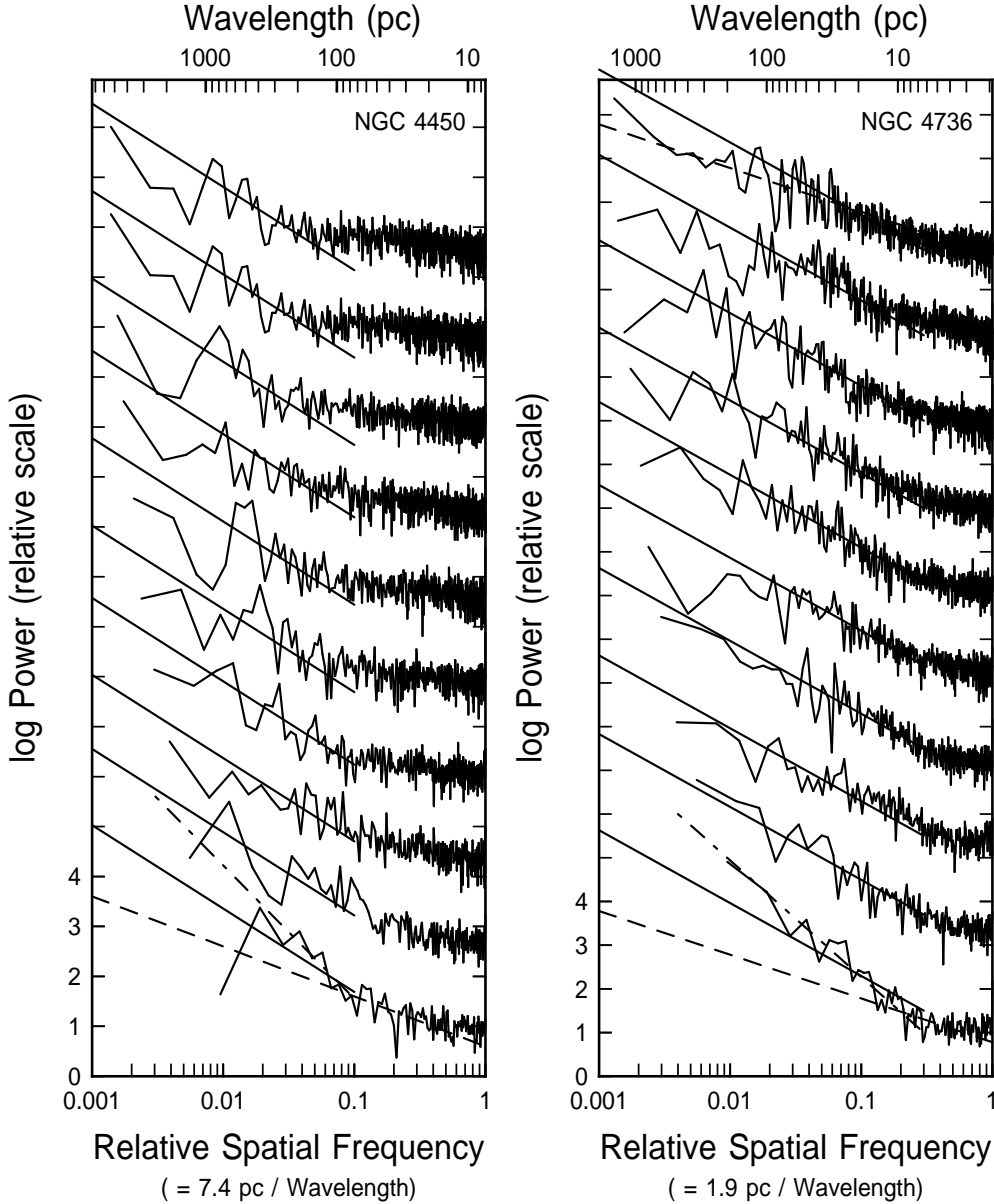


Fig. 10.— Fourier Transform power spectra of total intensity along the azimuthal scans shown in Fig. 10. The scans are stacked in order of increasing radius in the galaxy. The solid lines drawn through each scan have a slope of $-5/3$, the dashed line at the bottom and top has a slope of -1 , and the dot-dashed line at the bottom has a slope of $-8/3$. The similarity between the one-dimensional power spectra of dust spirals in these galaxies, the 1D power spectrum of HI emission on large scales in the Large Magellanic Cloud, and the 1D power spectrum of two-dimensional turbulence suggests that the spirals result from turbulent compression in a relatively thin disk.

Fig. 11.— The projected azimuthal scans used for the power spectra are shown superposed on the G4-G12 images. (See jpeg files in astro-ph.)

This figure "f1left.jpg" is available in "jpg" format from:

<http://arxiv.org/ps/astro-ph/0112527v1>

This figure "f1right.jpg" is available in "jpg" format from:

<http://arxiv.org/ps/astro-ph/0112527v1>

This figure "f3.jpg" is available in "jpg" format from:

<http://arxiv.org/ps/astro-ph/0112527v1>

This figure "f5.jpg" is available in "jpg" format from:

<http://arxiv.org/ps/astro-ph/0112527v1>

This figure "f6.jpg" is available in "jpg" format from:

<http://arxiv.org/ps/astro-ph/0112527v1>

This figure "f11left.jpg" is available in "jpg" format from:

<http://arxiv.org/ps/astro-ph/0112527v1>

This figure "f11right.jpg" is available in "jpg" format from:

<http://arxiv.org/ps/astro-ph/0112527v1>